Electronic Supplementary Material (ESI) for Energy & Environmental Science.

Supporting information for

Correlating the hydrogen evolution and zinc deposition/dissolution kinetics to cyclability of metallic zinc electrodes

Huijun Yang*, Yang Yang, Wuhai Yang, Gang Wu, Ruijie Zhu*

huijun0311@gmail.com

vjb92682@elms.hokudai.ac.jp

Materials

All materials used in this study were stored at room temperature, without any special considerations for storage. The heptahydrate salt, $ZnSO_4.7H_2O$, provided by Tokyo Chemical Industry, was mixed with deionized water to formulate a 2 mol L^{-1} $ZnSO_4$ (2M) for electrolyte solution. This solution was used for all test cells, except when explicitly mentioned otherwise. We measured the pH of the 2 mol L^{-1} $ZnSO_4$ electrolyte as 4.0, using a Lutron pH-208 pH meter.

We used GF/A glass fiber filters from Whatman-100, which we shaped into 16 mm diameter plates to function as separators, without additional treatment. High purity (>99.99%) zinc foil obtained from Nilaco Company (with a thickness of 100 µm) was used as well. It was polished to remove impurities and the oxide coating using ethanol solutions and then cut into 10 mm diameter plates, prior to electrochemical characterization.

Cell assembly and electrochemical characterization

The potentials used in this study were referenced to Ag/AgCl (in saturated KCl aqueous solution) in the three-electrode system and Zn/Zn^{2+} in the two-electrode system without further illustration. All testing CR-2032 coin-type cells (Hohsen Corp) used in this work were assembled in ambient environment without special attention. All the cells were remained on open circuit for 4 hours before electrochemical characterizations. The galvanostatic charge-discharge tests were carried out in battery tester system (Neware Technology Co.) at 25°C. The asymmetric Zn//Cu cells were assembled by stack of Zn plate, GF separator and Cu plate with 40 µL 2 mol L^{-1} $ZnSO_4$ aqueous electrolyte. The Zn reversibility in Zn/Cu cells was obtained from the capacity ratio of Zn stripping (controlled by cutoff potential of 0.5 V *vs.* Zn/Zn^{2+}) to Zn plating process (controlled by capacity, or the current density and time).

Linear sweep voltammetry measurement was carried out on an electrochemical workstation (Princeton VersaSTAT3). The three-electrode system is composed of Zn foil (counter electrode, CE), Ag/AgCl electrode (reference electrode, RE) and metal substrate plate (working electrode, WE, e.g. Cu plate), respectively. The Zn deposition/dissolution at different current densities, Zn plates were used as working and counter electrodes, with Ag/AgCl reference electrode. The Tafel curves was also obtained by three electrode system at the scan rate of 5 mV s^{-1}. The Electrochemical impedance spectra (EIS) of symmetric Zn cells were measured in Potentiostat/Galvanostat PGSTAT30, Autolab Co. Ltd., Netherlands with the frequency ranging from 100 kHz to 0.1 Hz. The amount of hydrogen evolution was analyzed by GC-MS measurement for a sealed cell after cycling at different current densities.

Characterizations

All the Zn electrodes after electrochemical studies were rinsed three times in dimethoxyethane (DME) solution to remove the precipitated salt residues in the surface. Prior to the characterizations, the samples were transferred to vacuum box to fully remove the DME solvent. (1) Scanning Electron Microscope (SEM) measurement and energy dispersive spectroscopy (EDS) measurement were conducted on ZEISS Sigma 500 machine. (2) The Raman spectra were performed by a JASCO microscope spectrometer (NRS-1000DT) and a Renishaw inVia microscope. The excitation light of an air-cooled He−Ne laser at 632.8 nm wavelength was focused on the electrode surface through a 50×long working distance lens (Olympus America Inc.). The confocal slit was adjusted to be 2.0 μm to minimize the band broadening effect due to the contribution of non-confocal signal. The scattered light was collected in a backscattering geometry along the same optical path as the pumping laser. The

spectral resolution of the Raman spectra in the study was ca. 1.0 cm^{-1}. (3) FTIR measurements were carried out on IRT-5200 Infrared Microscope spectrometer (JASCO Corp.). Typically, 64 interferograms were accumulated for one spectrum with a resolution of 4.0 cm^{-1}. For the etching process, the cycled Zn anode plate was assembled onto the sputtering target within an auto fine coater (JFC-1200, JEOL) in a vacuum environment (10~20 Pa, 10~15 mA current). The etching time was fixed at 10 s per time.

Computational Methods

COMSOL Multiphysics was used to simulate the concentration gradient. growth. Here, the flux of Zn^{2+} is controlled by Fick's law (Equation S1):

$$\frac{\partial c_{Zn^{2+}}}{\partial t} = \nabla \cdot (D \nabla c_{Zn^{2+}}) \quad \textit{(Equation S1)}$$

where c_{Zn2+} is the concentration of Zn ion, t is the time and D is the diffusion coefficient of the Zn ion, respectively.

Density Functional Theory (DFT) calculations for ESP of anions and binding energy among cations, anions and H2O were performed in Gaussian 16W software package. Geometrical optimization and frequency analysis adopted the B3LYP1 method with 6-311++G(d,p) basis sets. When the structure 3 involves Zn and I, the B3LYP method with def2tvzp basis sets was adopted.

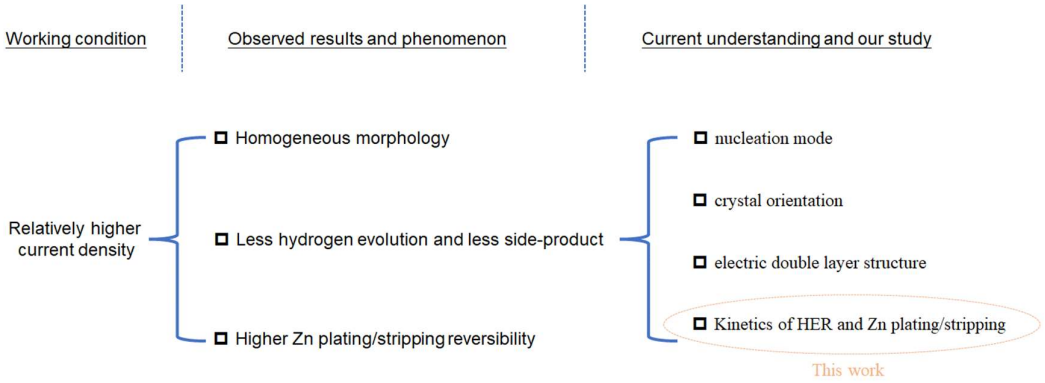

Fig. S1. Summary of the observed results and the current understanding on this topic.

Notes: The observed phenomenon of higher Zn plating/stripping reversibility at relatively higher current densities can be attributed to several factors, including nucleation mode, crystal orientation, and the structure of the electric double layer. It is important to note that changes in current density significantly alter the properties of metal electrodeposition, particularly in complex aqueous systems affected by the hydrogen evolution reaction. In our study, we have delved into both the kinetics of the hydrogen reaction and the Zn plating/stripping kinetics, aiming to provide fresh insights into this intricate battery system.

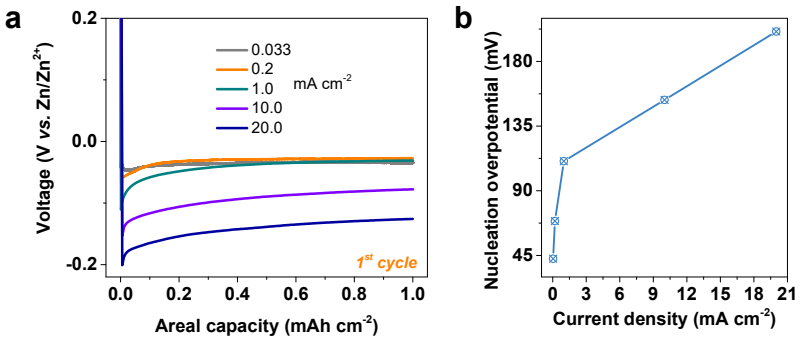

Fig. S2. (a) Potential evolution of initial cycle for the Zn//Cu cell working at different current densities. (b) The nucleation overpotential dependence on current density.

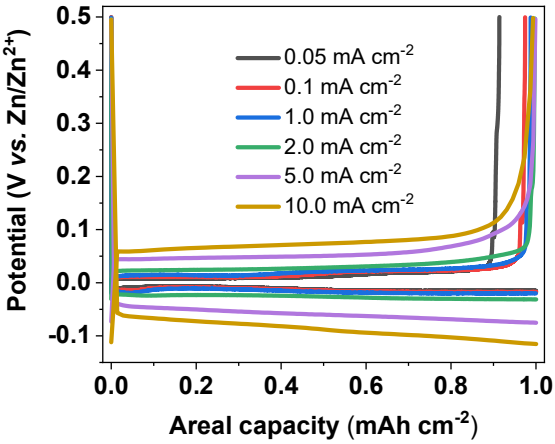

Fig. S3. Potential evolution of Zn//Cu cell working at different current densities.

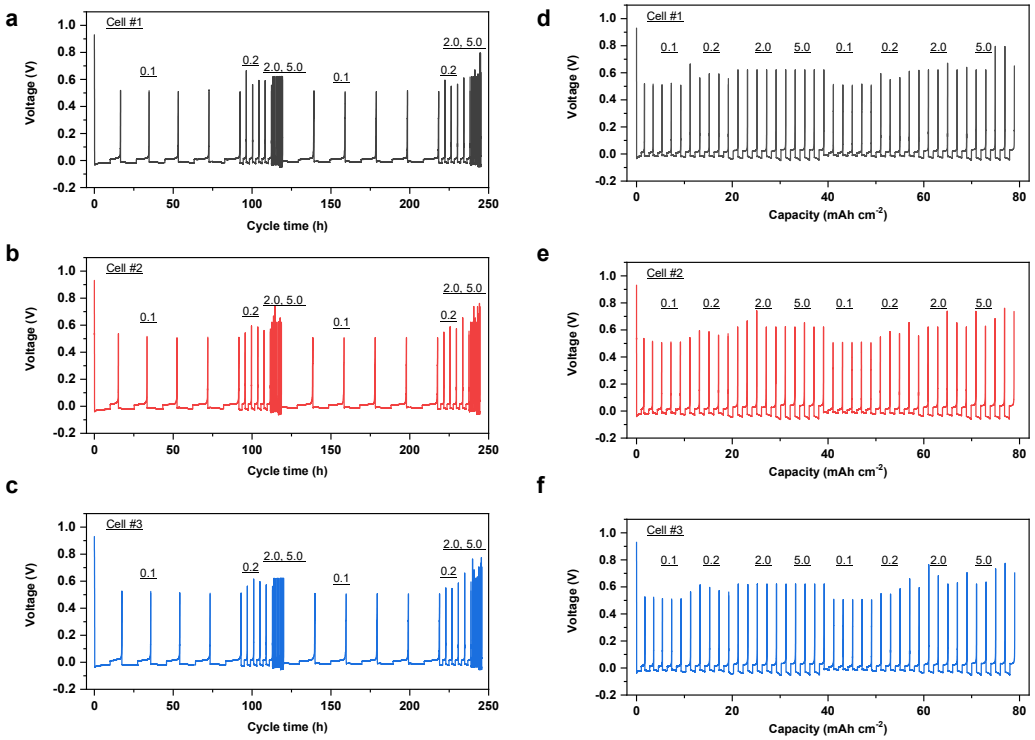

Fig. S4. Zn plating/stripping reversibility at the loop test of rate performance. (a) The corresponding potential evolution profile versus cycle time (b) the corresponding potential evolution profile versus capacity.

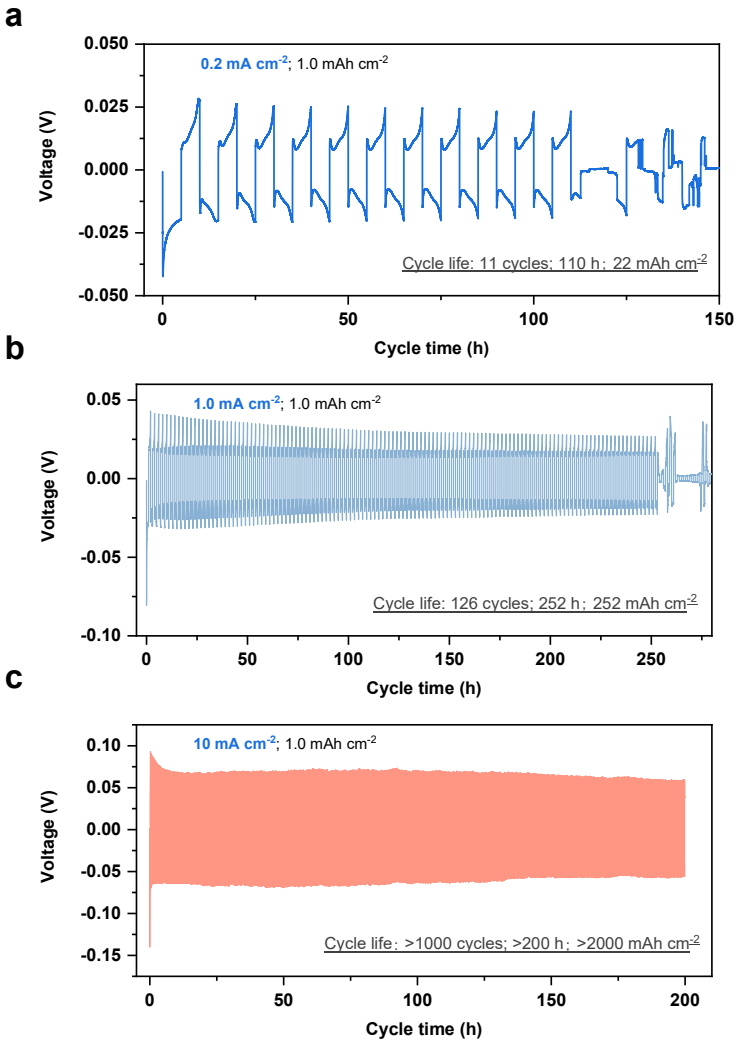

Fig. S5. Cyclic stability of Zn//Zn symmetrical cells at different current densities. (a) 0.2 mA cm^{-2}; (b) 1.0 mA cm^{-2}; (c) 10 mA cm^{-2}.

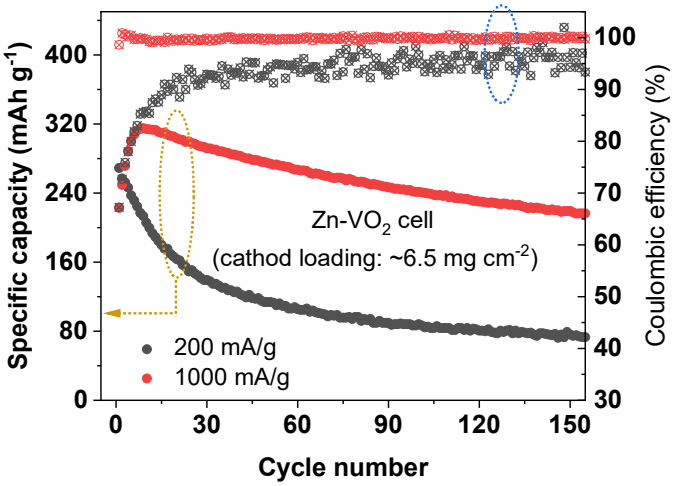

Fig. S6. Cyclic stability of Zn//VO_2 cells at different rates.

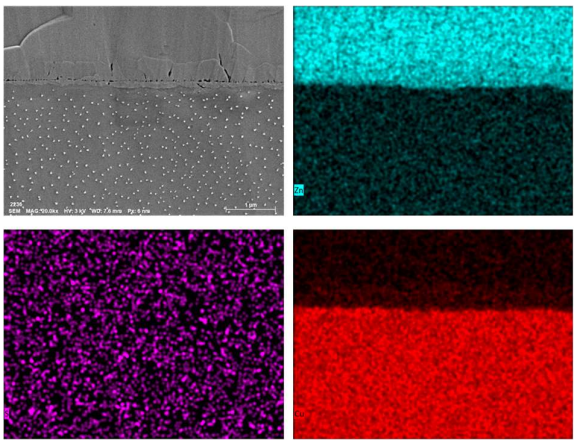

Fig. S7. Cross-section SEM images and its corresponding elemental mapping of Zn plating at high-C Zn plating.

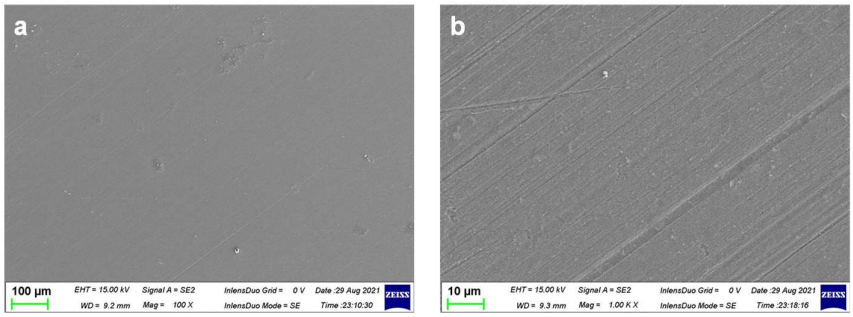

Fig. S8. Top-to-down view SEM images of Cu substrate after Zn plating/stripping at high-C.

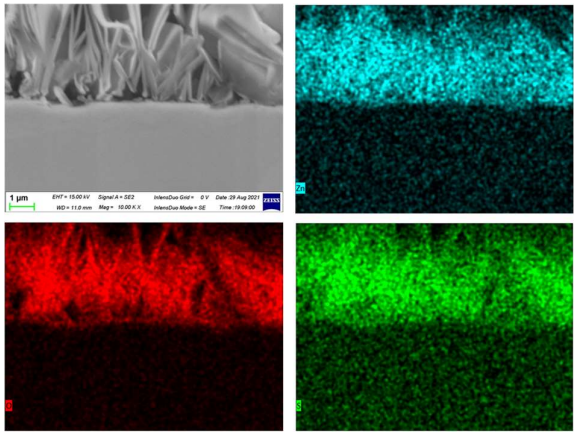

Fig. S9. Cross-section SEM images and its corresponding elemental mapping of Cu substrate after Zn plating/stripping at low-C.

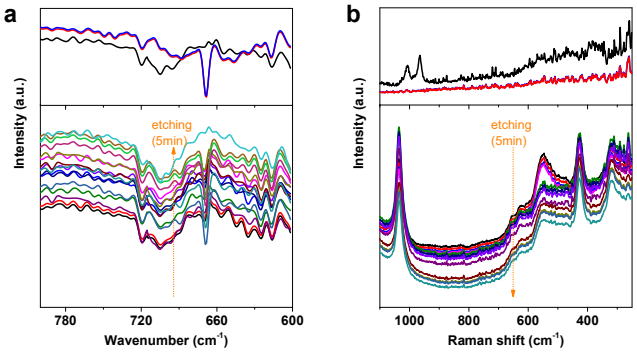

Fig. S10. Cu substrate surface component after Zn plating/stripping state (top: high-C, bottom: low-C) by (a) FT-IR spectra and (b) Raman spectra.

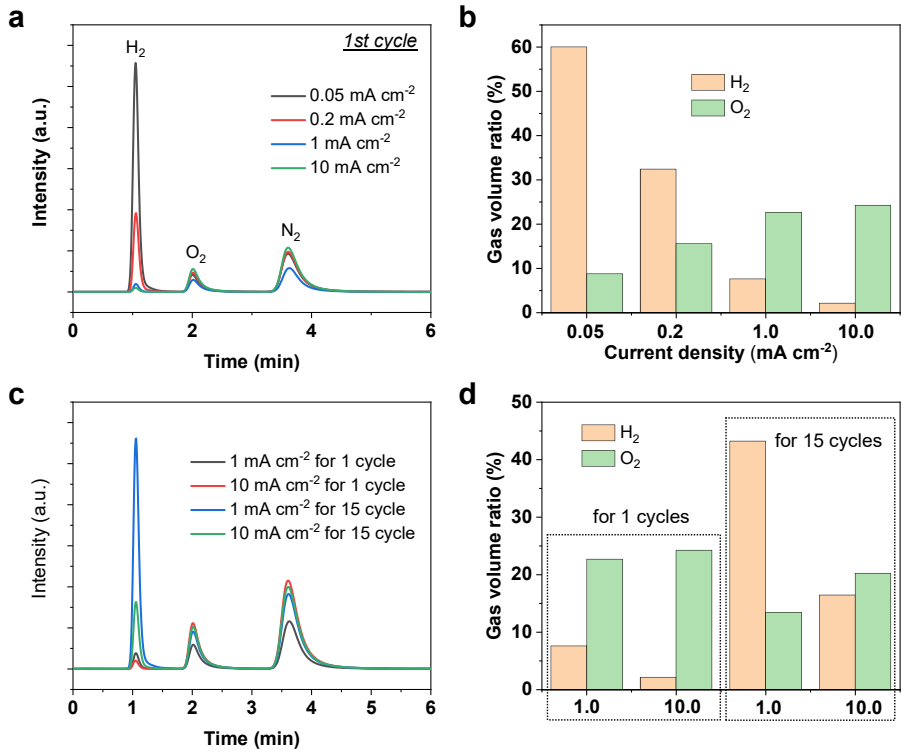

Fig. S11. GC-MS result of Zn plating/stripping under different current densities. (a) The relative intensity of gas evolution including hydrogen, oxygen, and nitrogen, respective. (b) The bar chart of gas volume ratio of hydrogen evolution under various current densities. (c) The relative intensity of gas evolution under different cycles. (d) The corresponding bar chart of hydrogen evolution.

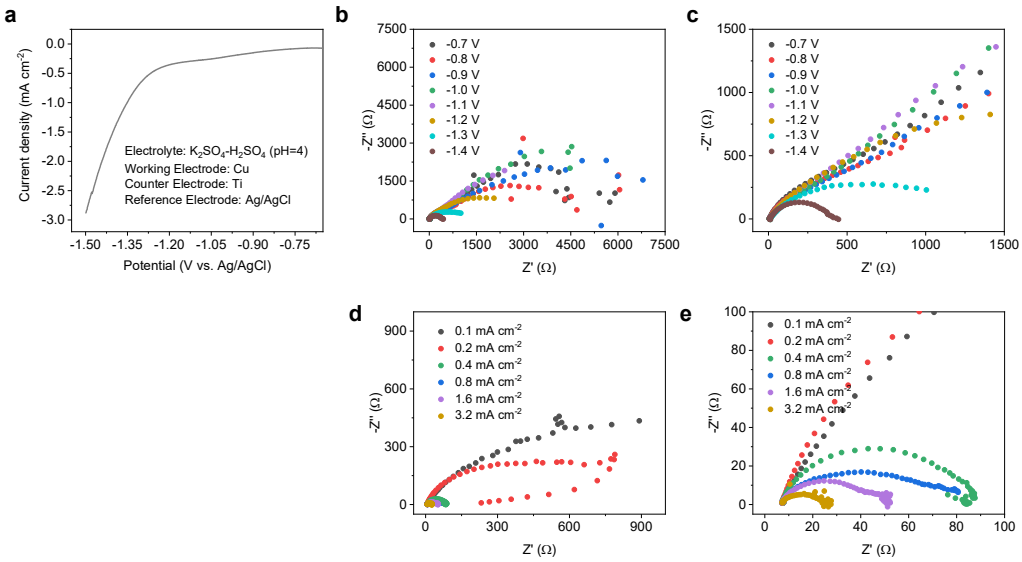

Fig. S12. EIS impedance profile of hydrogen evolution in the K_2SO_4-H_2SO_4 (pH=4) solution. (a) the linear sweep voltammetry profile of HER. (b-c) the charge-transfer impedance profile at different applied voltage. (d-e) the charge-transfer impedance profile at different applied current density.

Notes: In the three-electrode system, Ag/AgCl was used as the reference, and the electrolyte was confirmed as a K2SO4-H2SO4 (pH=4) solution, eliminating the interference of Zn reduction. Unlike the ZnSO4-based electrolyte, this selected electrolyte solely involved hydrogen evolution during the test (Fig. S12a). The charge-transfer impedance was characterized by the electrochemical impedance spectroscopy (EIS) profile at different applied voltages. We observed that the charge-transfer impedance (R_{ct}) gradually decreases with increasing applied voltage, consistent with fundamental electrochemical principles. At more negative potentials, the extensive accumulation and coverage of protons on the working electrode (a Cu plate in our study) enhances hydrogen evolution. Similarly, we further characterized the charge-transfer impedance at different current densities. As the current increases, the R_{ct} of HER decreases, which is caused by the potential shift, and the conclusion is consistent with the potentiostatic EIS tests and the fundamental electrochemical perspective. The increase of current density is seemed to promote the kinetics of HER, which is contrast with the case in Zn-based electrolyte. Therefore, we assume that the HER reaction kinetics in the Zn-based electrolyte is highly influenced by the kinetics of Zn/Zn^{2+}. It makes more sense that the decrease in the volume of hydrogen seen in the GC results is partially attributed to the change in the assistance with Zn reduction. Indeed, we have observed that the kinetics of both Zn plating/stripping and the hydrogen evolution reaction (HER) are intricately intertwined, making them challenging to distinguish using common characterization methods. We hypothesize that both reactions at the interface are predominantly dependent on the $Zn(H_2O)_6^{2+}$ species.

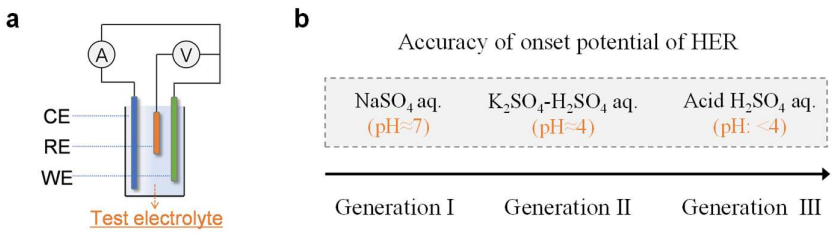

Fig. S13. Calibration of hydrogen evolution in the $ZnSO_4$ aqueous electrolyte. (a) the schematic illustration of three-electrode cell. (b) the used electrolytes to simulate the hydrogen evolution in $ZnSO_4$ aqueous electrolyte.

Note: The cathodic current in $ZnSO_4$ aqueous electrolyte generally combines the hydrogen evolution and the reduction of Zn^{2+}. These mixed two processes seem very difficult to decouple by common electrochemical characterizations. Therefore, some electrolytes have formulated to simulate the hydrogen evolution of $ZnSO_4$ aqueous electrolyte and eliminate the interference from reduction of Zn^{2+}. The first-generation electrolyte generally employed Na_2SO_4 aqueous electrolyte, which hardly reflects the true capability of hydrogen evolution of $ZnSO_4$. The second generation takes the H+ concentration as the major source of hydrogen evolution, however, still far from the true condition of hydrogen evolution, because of the major contribution of $Zn(H_2O)_6^{2+}$. Therefore, we recommend more acid H_2SO_4 aqueous solution should be employed to truly simulate the hydrogen evolution of $ZnSO_4$.

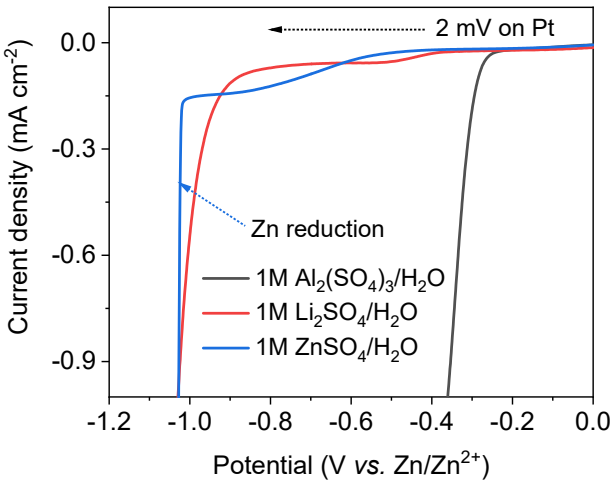

Fig. S14. The linear sweep voltammetry profile in the different electrolyte to study the effect of cations.

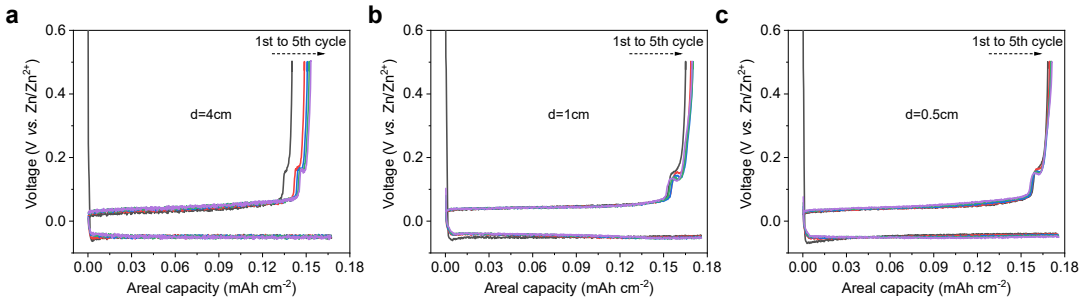

Fig. S15. The potential curves of Zn plating/stripping process in a large electrochemical breaker cell with different distance between Zn counter electrode and Cu working electrode. (a) distance=4 cm, (b) distance=1 cm, (c) distance=0.5 cm.

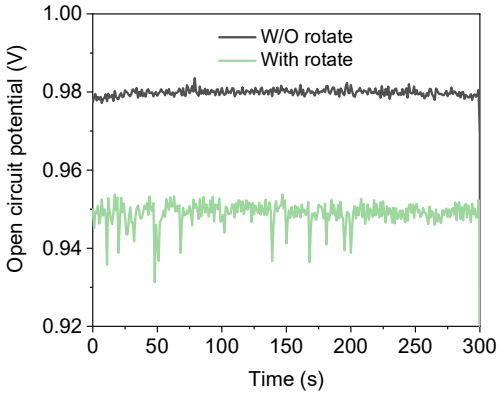

Fig. S16. The open circuit potential of Zn//Cu cells in the ZnSO4 electrolyte with or without rotate.

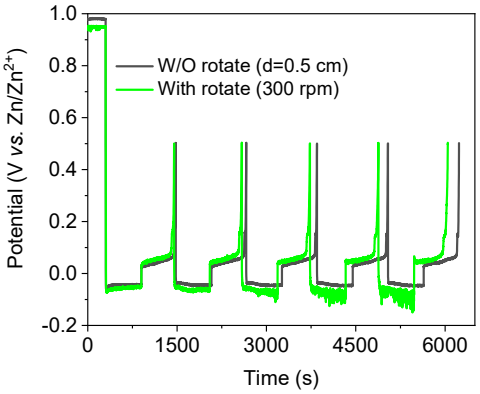

Fig. S17. The potential evolution of Zn plating/stripping in Zn//Cu cells with or without electrolyte stirring. The electrolyte stirring at 300 rpm is designed to eliminate the effect of concentration gradient.

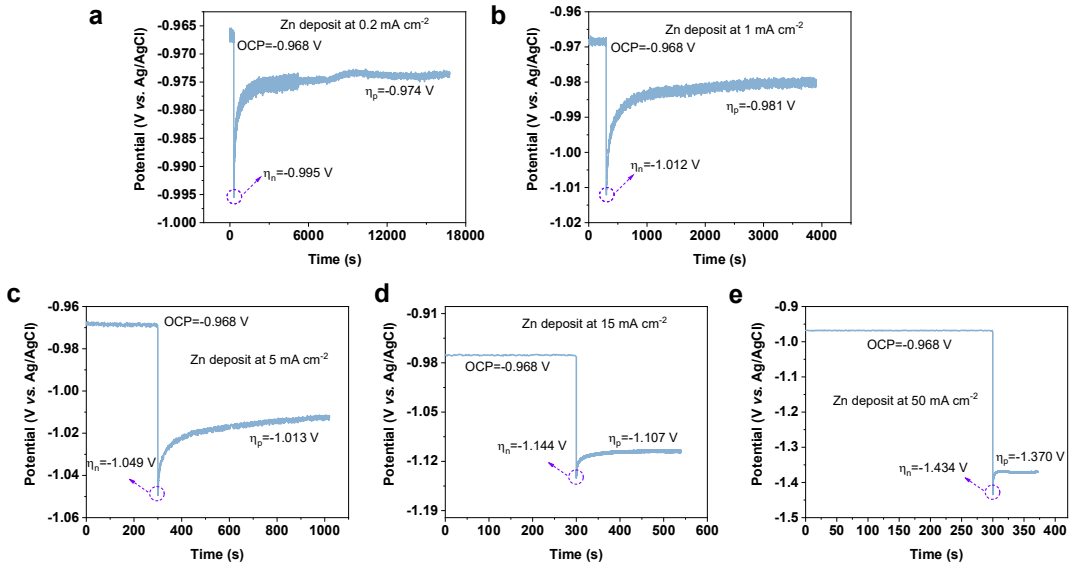

Fig. S18. The potential evolution of Zn plating at different current densities. Zn plates as both working and counter electrode. Ag/AgCl as reference electrode. The capacity is controlled as the same, 1 mAh cm^{-2}. (a) 0.2 mA cm^{-2}, (b) 1.0 mA cm^{-2}, (c) 5.0 mA cm^{-2}, (a) 15.0 mA cm^{-2}, (d) 50.0 mA cm^{-2}.

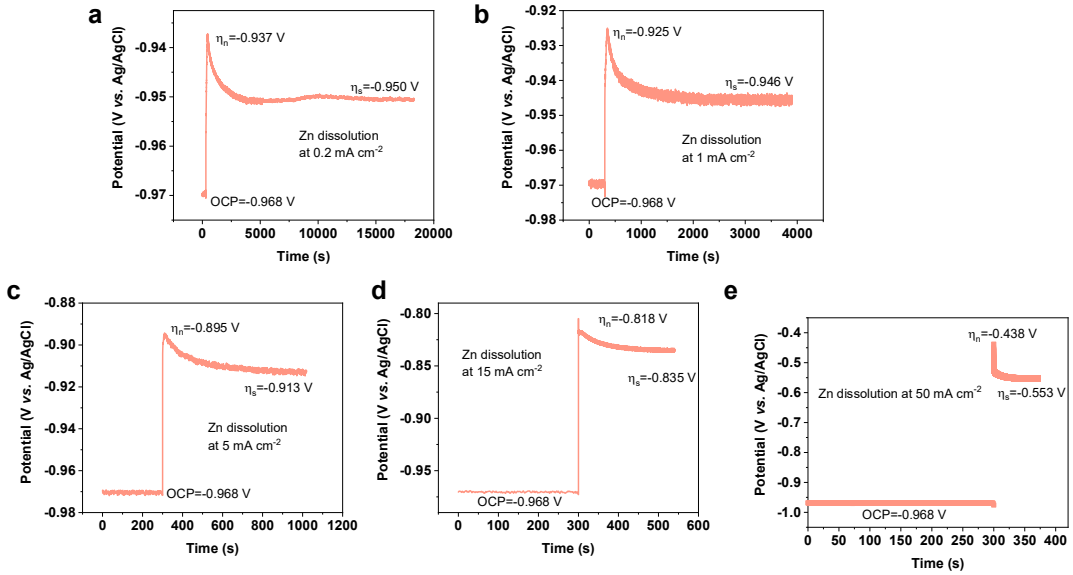

Fig. S19. The potential evolution of Zn stripping at different current densities. Zn plates as both working and counter electrode. Ag/AgCl as reference electrode. The capacity is controlled as the same, 1 mAh cm^{-2}. (a) 0.2 mA cm^{-2}, (b) 1.0 mA cm^{-2}, (c) 5.0 mA cm^{-2}, (a) 15.0 mA cm^{-2}, (d) 50.0 mA cm^{-2}.

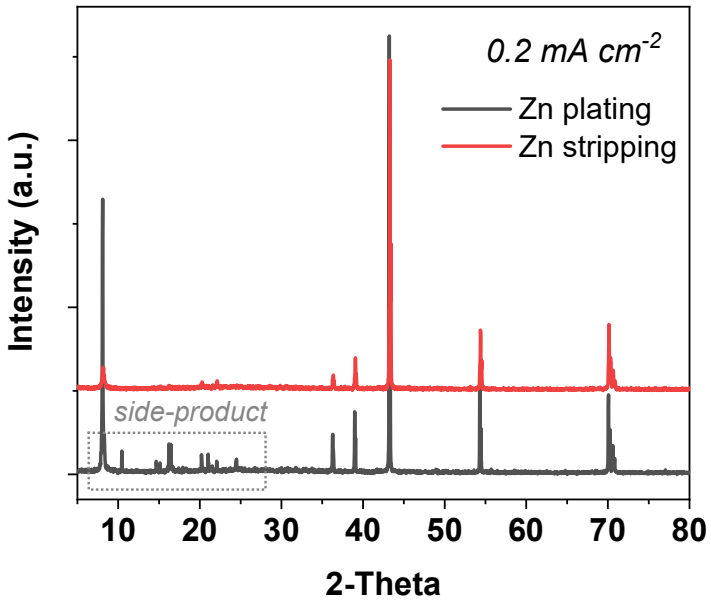

Fig. S20. XRD pattern of Zn plating and Zn stripping sample at low-C (0.2 mA cm^{-2}).

a

	Low current	High current
Zn nuclei density	Lower	Higher
Zn^{2+} concentration in the interface	Higher	Lower
HER substrate and hydrogen evolution rate	Cu, faster	Zn, slower
ZSH formation	Many	Few
Zn morphology and reversibility	Dendritic, lower	Uniform, higher

b

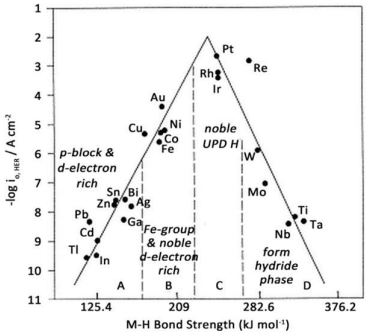

Fig. S21. (a) The summary of Zn plating/stripping at low and high current densities. (b) Volcanic curves of hydrogen evolution materials based on M-H bonding energy as logi0 value. Approximate location of graphite materials in volcanic curves by contrast with common metals of Zn, Cu, Ni and Ti metals. Modified with permission from ref.[1] Copyright 2000, Elsevier.

Note: The striking dependence of morphology on current density can be partially explained by the extension of the substrate effect. According to the classic volcano curve of hydrogen evolution materials, the Cu substrate shows lower overpotential to trigger hydrogen evolution than Zn metal.

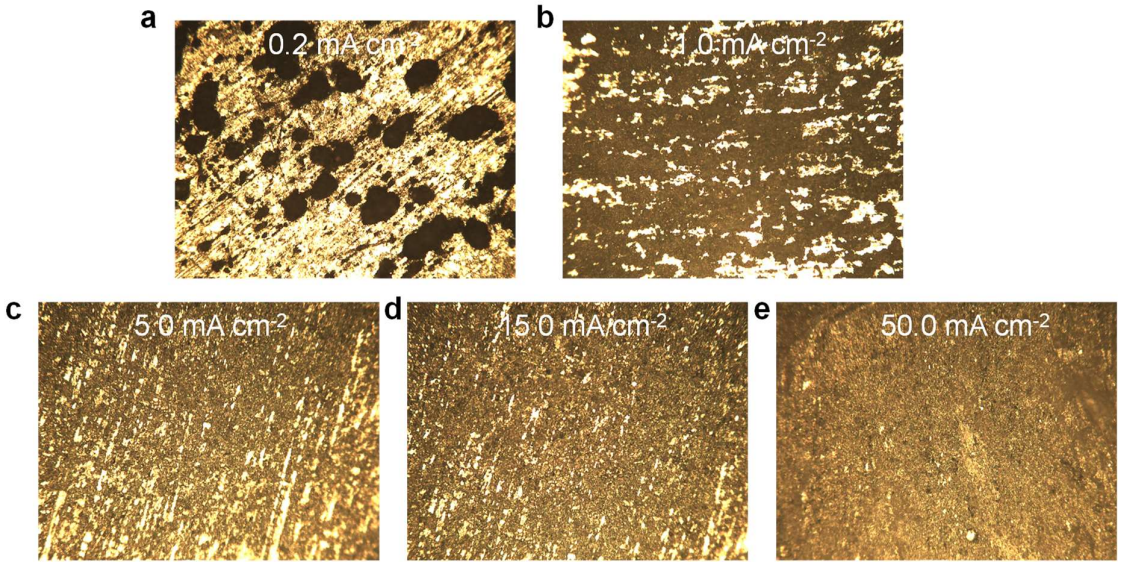

Fig. S22. Optical microscopy observation of Zn deposition samples at different current densities. (a) 0.2 mA cm^{-2}, (b) 1.0 mA cm^{-2}, (c) 5.0 mA cm^{-2}, (a) 15.0 mA cm^{-2}, (d) 50.0 mA cm^{-2}.

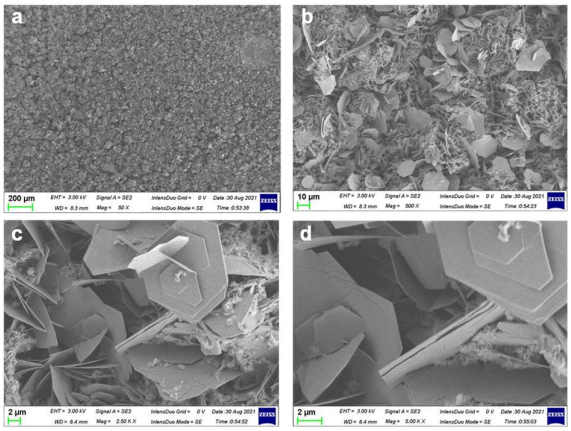

Fig. S23. (a-d) Top-to-down view SEM images of Zn plating on Ni substrate at low-C.

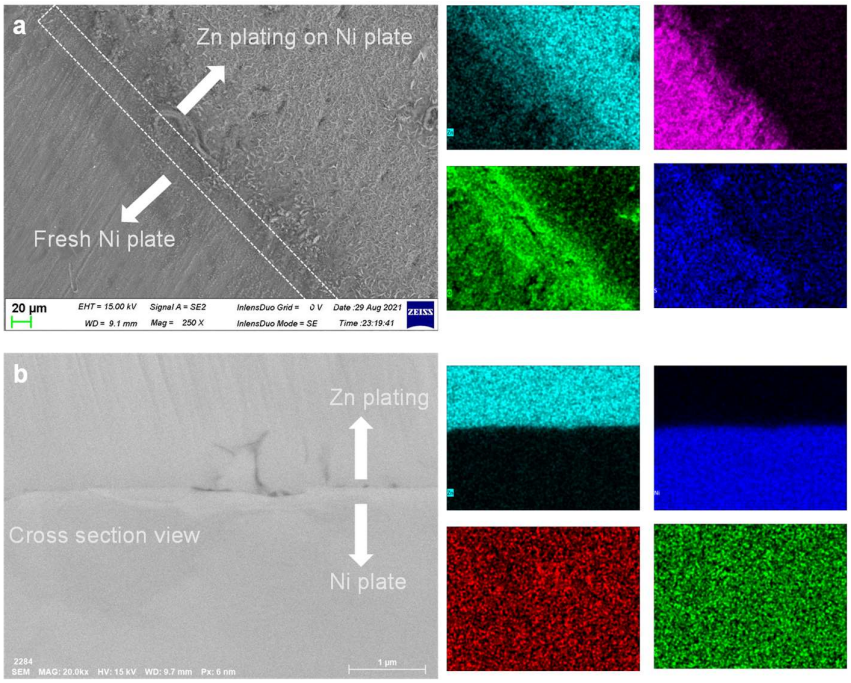

Fig. S24. SEM images and corresponding elemental mapping of Zn plating on Ni substrate at high-C. (a) Top-to-down view, (b) Cross-section view.

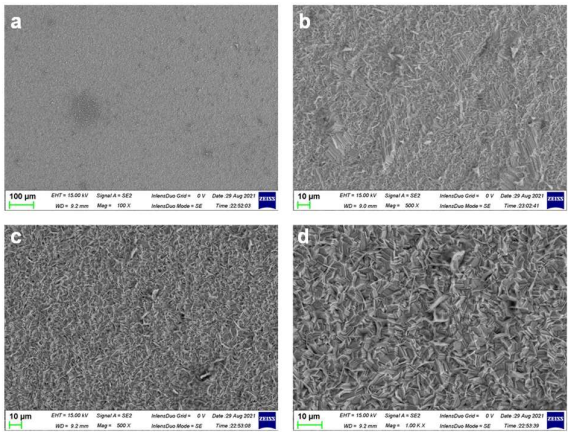

Fig. S25. (a-d) Top-to-down view SEM images of Zn plating on Ni substrate at high-C.

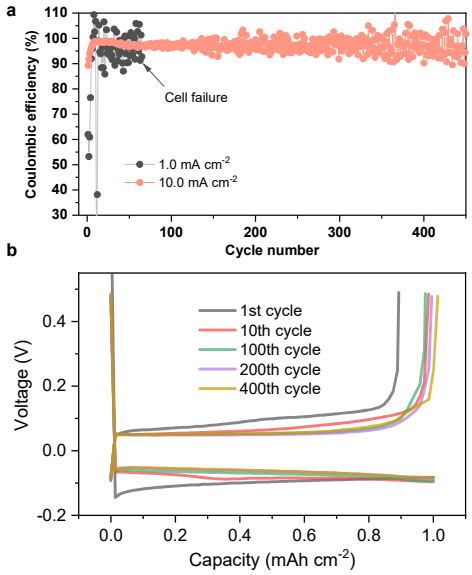

Fig. S26. Zn plating/stripping efficiency on SS substrate at different current densities (a) efficiency values, (b) the corresponding potential evolution at high-C.

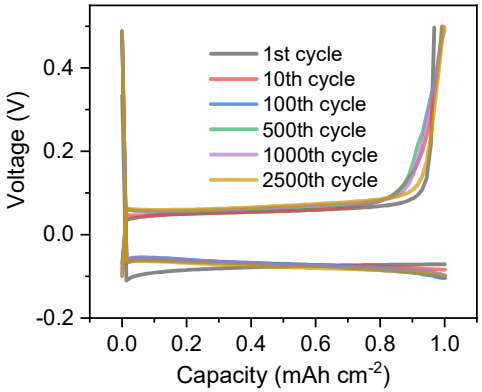

Fig. S27. The potential evolution of Zn plating/stripping on Ti substrate at high-C.

Table S1. The deprotonation energy via DFT computation in the aqueous environment.

$Zn(H_2O)_6^{2+}$	H^+	$Zn(H_2O)_5(OH)^+$	E (kJ/mol)
-2237.920164	-0.22518	-2237.493199	529.7865
H_2O	H^+	OH^-	
-76.452201	-0.22518	-75.969474	676.1896
H_3O^+	H^+	H_2O	
-76.847774	-0.22518	-76.452201	447.3668

Supplementary notes for the sample contamination in cross-section SEM

The cross-sectional polishing treatment was performed on a cryo-cross-section polisher (IB-19520CCP JEOL). This equipment is a cross-section polisher that performs cross-section milling of samples by Ar^+ beam irradiation with the addition of a cryo-function, enabling processing with reduced thermal damage caused by ion beams. Hence, the acceleration voltage can be up to 8 kV, and the etching rate is 3 to 4 times faster than that of the old type of cross-section polisher. However, this also leads to another problem, high-rate etching allows us to process thicker metal electrodes, but the material produced by etching can reattach itself to the sample surface because it cannot be removed from the vacuum chamber in time. This results in similar contamination on the surface of most of the samples that are polished at high-rates, which consists of elements from the metal foil itself, carbon, and some elements that may be left in the chamber.

Reference:

1. Conway, B. & Jerkiewicz, G. Relation of energies and coverages of underpotential and overpotential deposited H at Pt and other metals to the 'volcano curve'for cathodic H2 evolution kinetics. *Electrochim. Acta* **2000**, 45, 4075-4083.